Dynamic behavior of droplets impacting cylindrical superhydrophobic surfaces with different structures

Lijuan Qian[*, a, b](钱丽娟), Huang Cong [a](黄聪), Li Lv [a] (闾荔) , Qingfei Fu[c](富庆飞) ,Chao Fu[d] (付超)
a College of Mechanical and Electrical Engineering, China Jiliang University, Xueyuan Street,258, Hangzhou, 310018, Zhejiang, China
b Key Laboratory of Intelligent Manufacturing Quality Big Data Tracing and Application of Zhejiang Province, China Jiliang University, Hangzhou 310018, China
c School of Astronautics, Beihang University, Beijing 100191, China.
d SINTEF Energy Research Kolbjoern Hejes vei 1A, 7491 Trondheim, Norway
(*Electronic mail: qianlj@cjlu.edu.cn.)

Abstract: The dynamic behavior of droplets impacting cylindrical superhydrophobic surfaces with different structures (azimuthal groove, axial groove, pillar) is studied in this work. The rebound and splash thresholds with different structures were also proposed, which depended on D/D_0 (where D is the cylinder diameter and D_0 is the initial droplet diameter) and the surface structure of the substrate. Based on the energy conservation approach, a complete rebound threshold semi-empirical model is constructed for cylindrical superhydrophobic surfaces. The recovery coefficient is used to measure the energy loss during the droplet impacting the superhydrophobic cylindrical surface. At the same time, the energy loss was significant on the cylindrical superhydrophobic surface with different structures, and the surface structure of the substrate played a vital role in the energy loss of the collision process. Then a prediction formula for the maximum spread diameter on the cylindrical superhydrophobic surface with different structures is presented to understand the droplet collision behavior further. In addition, a level wing-like splash morphology could reduce contact time on grooved superhydrophobic surfaces. Based on the contact time ($(\beta_{a\max}/\beta_{z\max})^{1/2}\tau$) as a function of the Weber number, the azimuthal grooved structure surface has the least contact time.

INTRODUCTION

The dynamic behavior of droplets impacting solid substrates has been extensively studied, including spreading, splashing, and contact time. Researchers have explored the superhydrophobic surface because of its unique rebound property. The maximum spreading diameter, recovery coefficient, splash threshold, contact time, and other parameters in the collision process have been studied in detail.[1-5] Superhydrophobicity reduces the substrate surface's wettability by adding micro/nano structures on the substrate surface, and the contact angle between the droplet and the substrate surface would be exceeded 150°. Because of the low surface wettability has extensive application in anti-corrosion, anti-icing, self-cleaning, drag reduction, and other fields.[6-9] At the same time, with the development of micromachining technology, such as mechanical micromachining, physical micromachining, and chemical micromachining, micro-structured surfaces with superhydrophobicity have been used to study the dynamic process of droplet collision.

Past reports focused on the droplet impact dynamics on superhydrophobic surfaces with microstructures, which showed the influence of impact velocity[10, 11], contact angle[12, 13], the pitch of pillars[14], and droplet size from the Cassie to Wenzel wetting transition.[15] The transition affected the outcome of the droplet collision. K.malla et al.[16] investigated the effect of groove pitch and Weber number on the droplet collision process. As the increase of Weber number or the groove pitch, the droplets would shift from complete bounding to bounding with droplet breakup to no bounding. Liu et al.[17] discovered a unique rebound mechanism on superhydrophobic surfaces with lattices of submillimeter-scale posts decorated with nano-textures. Droplets spread on impact and then leave the surface in a flattened pancake shape without retracting. Contact time would reduce by a quarter for the complete rebound. Clanet et al.[8] studied the dynamic behavior of droplets on superhydrophobic surfaces. In conclusion, the maximum spreading diameter of droplets was $D_{max} = D_0We^{1/4}$ at low viscosity and wettability. A criterion was proposed to predict whether the spreading would be limited by capillary effect or viscosity.

In addition, many plants and objects had both curvature and superhydrophobicity in nature and industry, which made it necessary to understand the kinetic behavior of droplets on superhydrophobic substrate surfaces. For this reason, many researchers have conducted experimental and numerical simulations on the dynamic characteristics of superhydrophobic cylindrical surfaces. Khurana et al.[18] studied the impacting dynamics of droplets on wettability cylinders with different diameters, mainly in the wettability fraction, spreading factor, and liquid film thickness. Under the same impact Weber number, with the increases of cylinder diameter relative to the droplet diameter, the effect of curvature would decrease on the wetting fraction, spreading factor, and liquid film thickness. In contrast, the Weber number significantly affected the shape of liquid film, formation, and fracture. On the conservation of energy, an analytical expression for the evolution of liquid film thickness with time was proposed. Zhang et al.[19, 20] proposed a new dimensionless parameter $\alpha=We/D^*$ (ratio of inertial force to surface tension) to describe the dynamics of a droplet collision and used this parameter to distinguish between upward rebound and downward stretch. At the same time, the topological structure of the cylindrical surface caused the droplets to experience asymmetric spreading and contraction, which led to asymmetric rebound and breakup. Under the large impact Weber number, the splashing phenomenon first occurred in the azimuthal direction of the droplet. Based on D^* and Weber numbers, the splashing threshold of the two directions was proposed. To learn more about the dynamics of droplets on the surface of a cylinder, Jin et al.[21] considered the influence of temperature. It was found that the maximum spreading diameter of the droplet in the azimuthal direction was more significant than the maximum spreading diameter in the axial direction on the cylindrical superhydrophobic surface, and the temperature had an influence on the diffusion factor in the azimuthal direction. In addition, the contact time was also an essential parameter for studying the droplet collision process. Researchers studied the contact time of the droplet impacting the cylindrical superhydrophobic surface and proved that the contact time could reach the minimum when the droplet diameter was equal to the diameter of the cylinder[22]. Liu et al.[22] found that water droplets impacting echevaria leaves exhibit asymmetric bouncing dynamics. The echevaria leaves surface was investigated by lattice Boltzmann simulation and system experiment. It revealed that this novel phenomenon results from an asymmetric momentum and mass distribution that allowed preferential fluid pumping around the drop rim. The asymmetry of the bouncing led ~40% reduction in contact time. The effects of the diameter ratio of cylindrical glass and Weber number on the postimpact regime, contact time, maximum spreading factor, and splash threshold were investigated by Khanzadeh et al.[13] Found that contact time on the cylindrical surface was up to 50% less than the flat one. To reduce the contact time during the droplet collision, Abolghasemibizaki et al.[23] fabricated a superhydrophobic surface fully decorated with cylindrical ridges. The dates showed that regardless of the droplet location of the contact point, when the kinetic energy of the drop is sufficient to completely wet the ridges, the contact time reduces ~13% as the consequence of ~20% faster retraction. After Abolghasemibizakiet et al.[24] designed a ribbed surface with additional macrotexture and found that ribbed macrotexture could further reduce the contact time. In the study of non-Newtonian fluids, Ranjan Mishra et al.[25] reported the post-collision elasto-hydrodynamics of non-Newtonian elastic or Boger fluid droplets (polyacrylamide (PAAM)) solution in water on convex or cylindrical targets of various diameters. Both hydrophilic and superhydrophobic surfaces were studied to deduce the role of wettability. In the case of superhydrophobic surfaces, PAAM droplets rebound at larger cylindrical diameters and higher Weber numbers compared to water. In addition, a summary of the great experimental was given for the droplet impact on cylindrical superhydrophobic surfaces in the appendix, as shown in Table 2.

The emergence of numerical simulation deepens the insights in the mechanism and dynamic behavior of droplet collision. Khojasteh et al.[26] used the numerical algorithm of level set-VOF to investigate the impacting process and found that under the same impact conditions, the maximum spread area on the spherical surface was greater than that on the plane surface, and gravity played a more critical role on the curved surface. Li et al.[27] adopted the improved

Boltzmann method to consider the droplet's eccentricity (β) to the cylinder's axis, surface wetness, viscosity ratio (λ), and other parameters. In case with $\lambda <1$, the viscosity ratio plays a minor role in the thickness variations of the deposited liquid, which decreases to a nonzero constant eventually; while for $\lambda>1$, the increase of the viscosity ratio significantly accelerates the decrease of the deposited liquid, and finally no fluid deposits on the cylinder. Wang et al.[28, 29] found that the droplets separated and recombined at the bottom of the cylinder when impacting the cylindrical hydrophilic surface through a particle-based mesh-free numerical approach. On the hydrophobic surface of the cylinder, the droplets remain separated at the bottom of the cylinder after separation. The maximum axial spreading diameter increased with the increase of droplet impact velocity. In the rebound morphology, the contact time increased with the impact velocity and decreased with the impact velocity. Surface wettability is an important factor affecting droplet dynamics. Liu et al.[30] used a coupled level set and volume-of-fluid method and found that the worse the surface wettability was, the easier the liquid film rebounds. The maximum spreading diameter increases with the increase of the impact velocity. A method with a rectangular ridge decorated on the cylinder is proposed by Zhang et al.[31] to suppress and prevent the re-touch. With a small ridge height, the rebound pattern is changed from the intact re-touch rebound to the separate re-touch rebound, and the contact time is significantly reduced. Andrew et al.[14] used Lattice Boltzmann method and found that the anisotropic curvature of the surface was responsible for the contact time reduction. With the increase of curvature, the contact time is reduced. Moreover, the obstacle shape would impact the bouncing, particularly for larger obstacles. In brief, a summary of the great numerical simulation is given for the droplet impact on cylindrical superhydrophobic surfaces in the appendix, as shown in Table 3.

Although the dynamic behavior of droplets impinging the micro-structured surfaces and cylindrical surfaces has been widely studied, but the dynamic behavior of droplets impinging on the surface of a cylindrical structure was rarely studied. Therefore, cylindrical surface structures, including cylindrical pillar structure, azimuthal groove cylindrical structure (the groove is perpendicular to the cylinder's axis), axial groove cylindrical structure (the groove is parallel to the axis of the cylinder) were designed in this work to explore the influence of cylinder surface on dynamic droplet behavior.

EXPEIMENTAL AND MATERIAL

A: Surface preparation

In this work, cylindrical brass material with a diameter of 20±0.02mm, and precision CNC machining tools were used to make the cylinder azimuthal groove cylindrical surface, axial groove cylindrical surface, and cylindrical pillar surface, respectively. These three structural dimensions were 0.4±0.02mm, including the ridge width (w_1 or w_3), the groove width (w_2 or w_4), and the groove height(h), it was shown in Fig. 1b)-1),1b)-2),1b)-3). A commercial nano-coating (Never Wet, Ultra Every Dry, NC319, Made in China) is used to achieve superhydrophobicity on the cylindrical surface. The nano-coating treatment process mainly includes cleaning, impregnation, and drying. The specific process is as follows: (i) The surface of the brass structure cylinder was cleaned for 20 min by using an ultrasonic cleaning machine, repeated twice, and then washed once with deionized water to ensure a clean substrate material. (ii) The substrate material was placed for 5–7 min in a desiccator chamber (70°C) to ensure that the material was dry and non-oily. (iii) A superhydrophobic coating was evenly sprayed on the surface of the brass cylinder, which was then dried in a drying chamber (60°C-80°C) for 8–10 min. (iv) These steps above were reported three times to ensure the superhydrophobicity of the substrate material. The microscopic morphologies of the superhydrophobic surfaces, obtained through the above steps, are shown in FIG.1e. The ESEM (environmental scanning electron microscopy) image shows that the cylindrical surface is uniformly covered with silica nanoparticles.

The surface wettability was determined by measuring the static and the dynamic contact angles of water drops (16μL) on a flat brass groove substrate and pillar substrate using a standard contact angle goniometer ((JY-82B Kruss DSA), as shown in Fig.1c). The contact Angle was measured by the droplet method and the measurement error was ±2.5°, as shown in the first illustration presented in Fig.1c). The dynamic contact angles, including advancing and receding angle, were measured using injecting liquid to the drop or sucking liquid from the drop [shown in the second illustration presented in Fig.1c)]. The static contact angle of the superhydrophobic groove is θ=158°±2.5°, and the advancing, receding angles and sliding angels are θ_a =7°±2.5°, θ_r = 82°±2.5°, θ_s=8.5°±2.5°, respectively. These values were averaged over five measurements.

B: Experimental setup

In this experiment, the room temperature was ~20°C, and the relative humidity was ~50%. The experimental setup is shown in Fig.1a). The experiment was repeated five times for each view (cross view, front view, side view) with a camera under the same Weber number (same height condition). The liquid was using deionized water (the density (ρ) is 1000kg/m^3 and the surface tension (σ) is 0.072m/N), and the droplets are produced by a syringe pump (LSP02-1b). The average droplet diameter D_0 values were 2.4mm±0.02 mm, 3.1mm±0.02mm, 3.9mm±0.02mm, and 4.8mm±0.02mm. The droplet diameter, sample parameters, and experimental parameters are shown in table 1. Droplets were dropped from different heights and fell into the center of the cylinder surface. The impacting velocities ranged from 0.31 m/s to 1.9 m/s, corresponding to Weber numbers ranging from 3 to 150. Here, $We=\rho D_0 U_0^2/\sigma$ is the Weber number, representing the ratio of the inertia force and surface tension (where D_0 is the drop diameter, ρ is the liquid density, U_0 is the impact velocity, and σ is the liquid-gas surface tension).

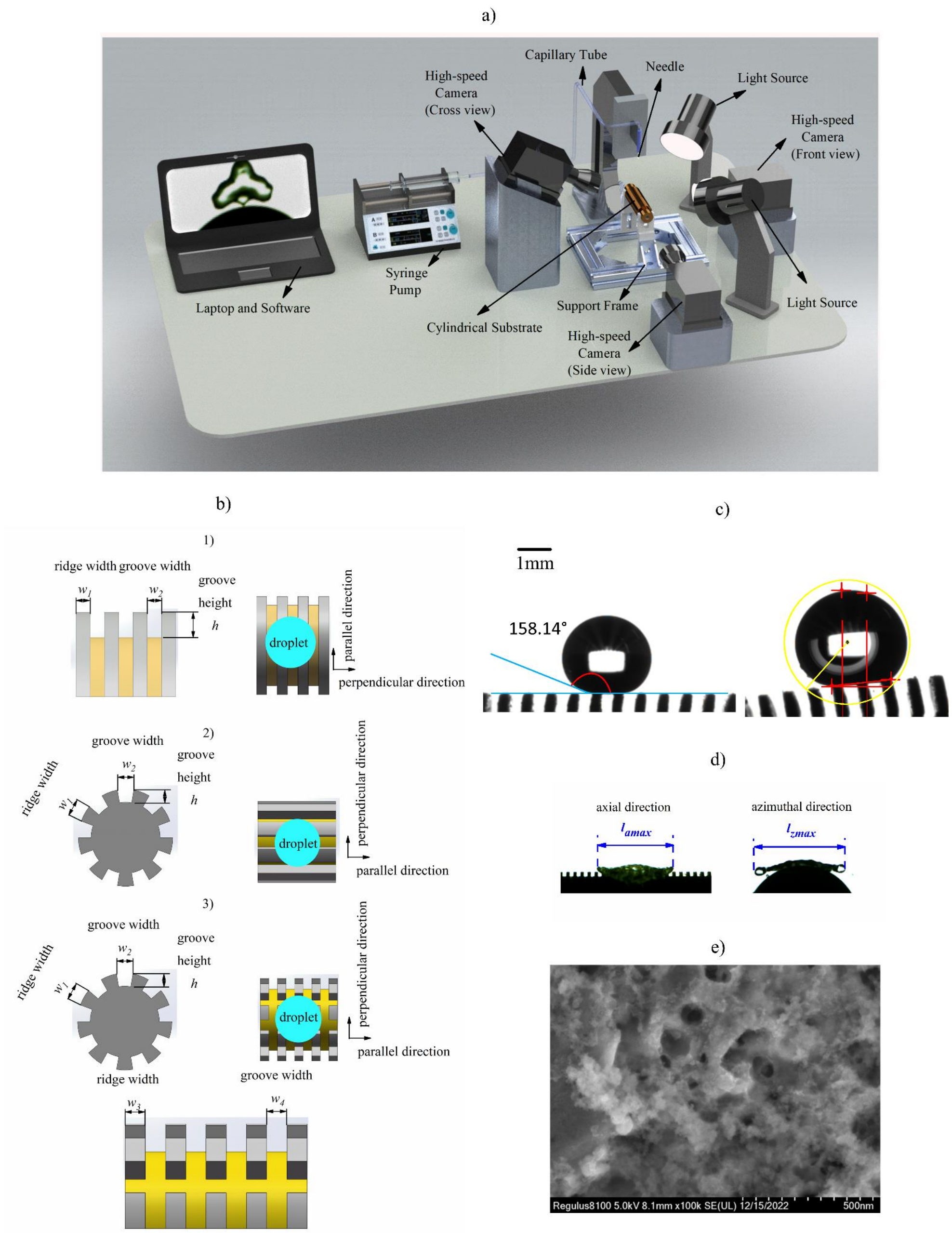

Fig.1. Schematic of the a) experimental setup, b) Schematic view of the micro-groove-liked texture cylindrical surface, 1) azimuthal groove cylindrical surface, 2) axial groove cylindrical surface, 3) pillar cylindrical surface. c) The static and dynamic

contact angles, and d) the maximum spreading diameter in the axial and azimuthal direction. e) Environmental scanning electron microscopy (ESEM) image of the cylindrical superhydrophobic surfaces.

The droplet collision process was captured using a high-speed camera (Fastcam Mini AX 100-C), a microscopic lens, and a stroboscopic LED spotlight which is the no-stroboscopic white light source. A high-speed camera (FASTCAM Mini AX Type 200K-C-32GB) frame rate of 4000 fps and shutter speed of 1/4000 was employed; Photos were taken from the front view, left view, and cross view (the angle between the camera and the horizontal plane is ~75°). Due to the angular differences in the crossed views, experimental data (the rebound threshold, contact time and maximum spread diameter) are obtained from the side view and the front view in this paper. The cross-sectional view is used to determine the morphology and process of droplet spreading. To ensure the repeatability of the experiment, the experiment was repeated five times for each condition. After each experiment, the substrate was dried using an air blower to remove the residue of water drops.

Table 1: Experimental conditions.

$We = \rho U_0^2 D_0 / \sigma$, $D^* = D / D_0$, $\rho = 1\times10^3 (\mathrm{kg/m^3})$, $\sigma = 7.2\times10^{-2} (\mathrm{N/m})$, $\beta_{z\max} = l_{z\max} / D_0$, $\beta_{a\max} = l_{a\max} / D_0$

D (mm)	D_0 (mm)	Drop height (mm)	Weber number
20	2.4, 3.1, 3.9, 4.8	4–200	3-150

Result and Discussion

A: Droplet Rebound

A high-speed camera (Fastcam Mini AX 100-C) is used to capture the droplet rebound process from the front, side, and cross views. As shown in Fig.2, the droplet underwent three processes after impinging the substrate surface: first spreading(0-5ms), then receding (5ms-12.5ms), and finally rebounding(12.5ms-15ms). In Fig. 2a, droplets' spreading and receding processes were relatively stable on the cylindrical superhydrophobic surface. The surface instability was almost non-existent, and the energy loss was slight. Surface tension and viscous force played a significant role in the collision, and droplets were not prone to splash. Therefore, the Weber number of the complete rebound of droplets on the cylindrical superhydrophobic surface was the largest. However, on the axial groove, azimuthal groove, and pillar cylindrical superhydrophobic surface, as shown in Fig. 2b, 2c, and 2d, there were unstable waves and disturbance phenomena on the surface of the droplet during the collision process. Especially in the process of receding (5ms-12.5ms), there was oscillation on the droplet's surface, the surface instability was more violent, and the energy dissipation was more significant during the contraction process. Therefore, compared with the cylindrical surface, the maximum Weber number of complete rebounds is slightly lower. A classical approach is used to understand the dynamics of liquid droplets. Under the situation of the diameter ratio ($4<D^*<9$) and Weber number ($3<We<150$), the complete rebound threshold (the droplet that could completely rebound without breaking during the collision) of cylindrical superhydrophobic surfaces with different structures is shown in Fig.3. It was found that the complete rebound threshold was different on the cylindrical superhydrophobic surface with different structures. The Weber numbers of complete rebounds were ~17 and ~21 on the azimuthal groove cylindrical superhydrophobic surface and axial groove cylindrical superhydrophobic surface, and the rebound threshold did not change with the changing of D^*. However, the maximum Weber number of complete rebounds was ~58 on the pillar cylindrical superhydrophobic surface, and the maximum Weber number of complete rebounds decreased with the increase of D^*. Finally, the maximum Weber number of complete rebounds of the cylindrical superhydrophobic surface was ~84. With the increase of D^*, the maximum Weber number of complete rebounds increases gradually. This was because the rebound of the droplet depends on the energy loss when the remaining kinetic energy can overcome the dissipated energy in the contraction process.[32-34]

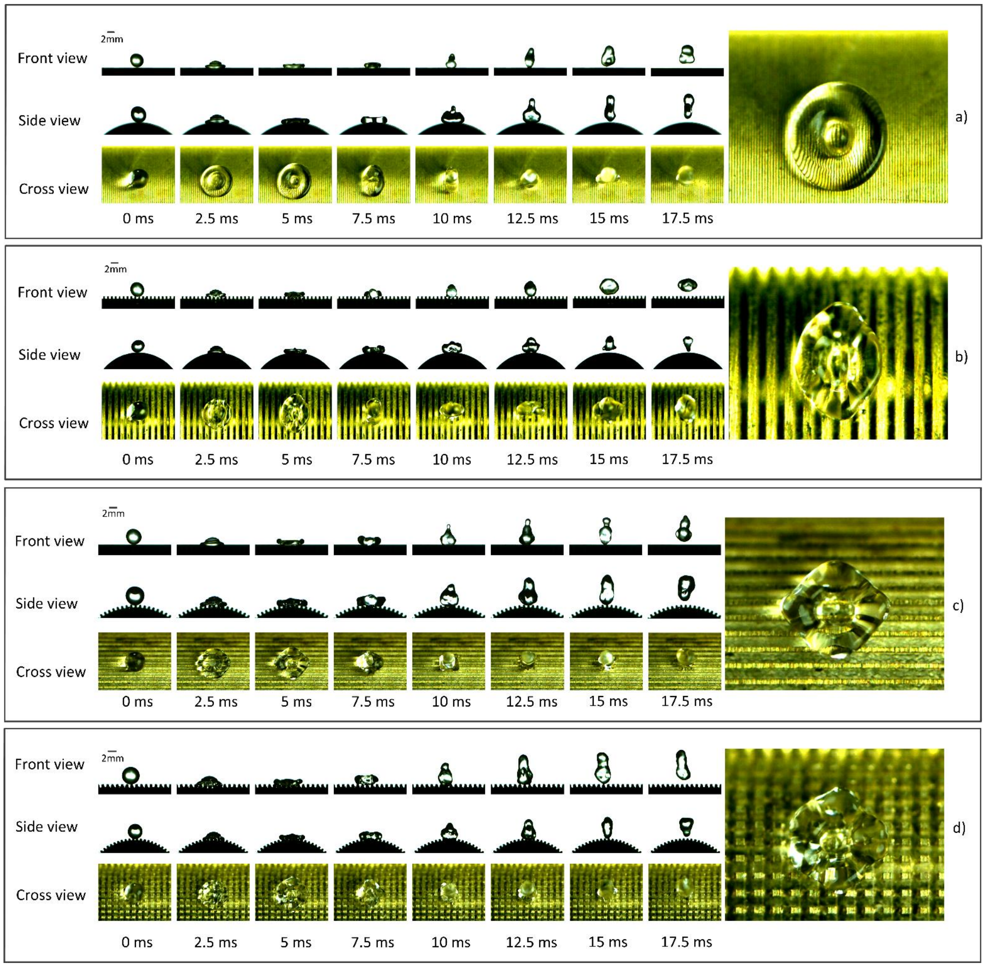

Fig.2. Schematic diagram of rebound morphology on superhydrophobic cylindrical surfaces with different structures. a) *We*=16, *D**=6.44, rebounding off the cylindrical superhydrophobic surface b) *We*=16, *D**=6.44 rebounding of the azimuthal groove cylindrical superhydrophobic surface c) *We*=16, *D**=6.44 rebounding of the axial groove cylindrical superhydrophobic surface d) *We*=16, *D**=6.44 rebounding of the pillar cylindrical superhydrophobic surface. Each image's first, second, and third rows represent high-speed snapshots selected from the front, side, and cross views.

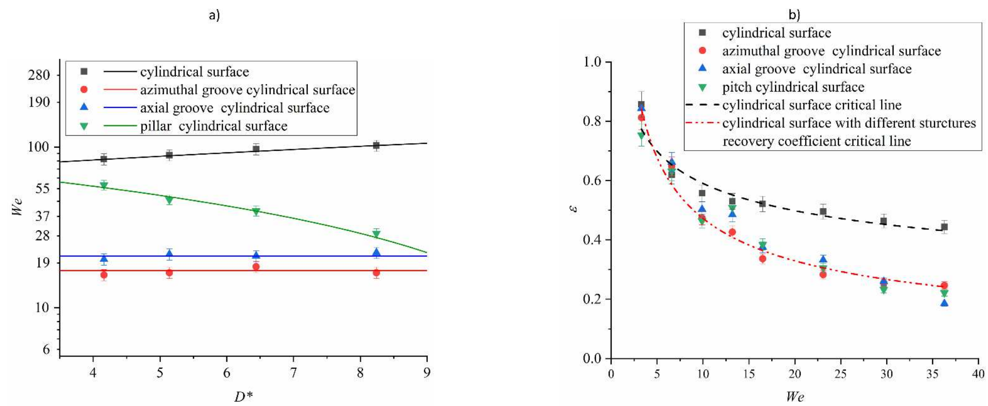

Fig.3. a) Diagram of the *We*-*D**, rebound threshold of cylindrical superhydrophobic surfaces with different structures, the black square, red circle, blue triangle, and the green inverted triangle represent the cylindrical surface, azimuthal groove cylindrical surface, axial groove cylindrical surface, and cylindrical pillar surface. b) At D^*8.24, the critical lines are the recovery coefficient (ε) of the cylindrical superhydrophobic surface with different structures, the black dashed line, and the red double dotted line.

To better understand the rebound threshold difference in different structure surfaces, the variation curve of the recovery coefficient with the Weber number is plotted to describe the energy loss of the collision. The restitution coefficient ($\varepsilon = V_1/V_2$) where V_1 is the velocity of the droplet when it first touches the substrate, and V_2 is the velocity of the droplet when it leaves the substrate. From the black dotted line (cylindrical surface critical line) and red double dotted line (cylindrical surface with different structures critical line) in Fig. 3b. When We>10, on the cylindrical superhydrophobic surface with structures, the restitution coefficient was significantly lower than that on the cylindrical superhydrophobic surface. This indicated that the droplet's energy loss during the collision was relatively significant on the structure surface. In this process, the droplet was in the Wenzel state, and the droplet filled the basal groove and had to overcome more barriers in the contraction process, so more energy was dissipated.[35, 36] At the same time, there were significant disturbance and instability waves on the surface of the droplet when the droplet impacted the structured substrate. With the increase of Weber number, the inertial force overcomes the surface tension of the droplet at larger impacting velocities, and the droplet was more likely to splash and break. The broken droplet would take away some droplet energy which decreases the droplet recovery coefficient.

In addition, the trend of the maximum spreading diameter with Weber number (We<40) was made for different structures. Here the axial and azimuthal maximum spreading diameters as l_{amax}, l_{zmax} in Fig.1d, and the corresponding non-dimension maximum spreading diameters$\beta_{xmax}=l_{amax}/D_0$ and $\beta_{zmax}=l_{zmax}/D_0$ is defined (where D_0 is the diameter of droplet). Previous studies have shown that droplet spreading is mainly affected by impact velocity, surface shape, and surface structure. On the cylindrical superhydrophobic surface, the topology of the cylinder droplets distributed more momentum in the azimuthal direction, making droplets spread more. The results showed that the maximum spreading diameter of droplets is closely related to the substrate structure, and the groove structure could certainly facilitate or hinder the spreading of droplets. Comparing Fig. 4,5, and 6, it is found that the maximum spreading diameter of droplets is significantly limited in the direction perpendicular to the groove structure, and the maximum spreading diameter of droplets is somewhat promoted in the direction parallel to the groove. When the droplet collides with the substrate surface, the droplet fills the inside of the groove, and the movement of the droplet is restricted in the direction perpendicular to the groove. This is because the surface energy of the liquid caught in the inner part of the groove could not be converted into kinetic energy at all. However, in the direction parallel to the groove, the surface energy of the droplet is more easily converted into kinetic energy. Thus, the spreading of the droplet is promoted. It could be concluded that the groove surface has anisotropic wettability, which significantly affected the maximum spreading diameter. In addition, a linear or exponential fit was used to obtain a prediction formula for the dimensionless maximum spread diameter with different structures. The prediction equations were also illustrated to predict the spreading during droplet collision. The error of fit is approximately 5%. The experimental error in the data is the measurement error, which totals approximately 3%. The total cumulative error in these equations does not exceed 10%.

Azimuthal groove cylindrical surface of maximum spread diameter prediction formula:

$$\beta_{x\max} = 1.75\left(\frac{D}{D_0}\right)^{-0.2} We^{\left(0.14\frac{D}{D_0}\right)^{-0.4}} \tag{1}$$

$$\beta_{z\max} = \left(1.95 - 0.1\frac{D}{D_0}\right) + 0.04We \tag{2}$$

Axial groove cylindrical surface of maximum spread diameter prediction formula:

$$\beta_{x\max} = 1.25 + 0.03We \tag{3}$$

$$\beta_{z\max} = \left(1.72 - 0.08\frac{D}{D_0}\right)We^{0.12} \tag{4}$$

Pillar cylindrical surface of maximum spread diameter prediction formula:

$$\beta_{x\max} = 1.25 + 0.02We \tag{5}$$

$$\beta_{z\max} = \left(2 - 0.1\frac{D}{D_0}\right) + 0.025We \tag{6}$$

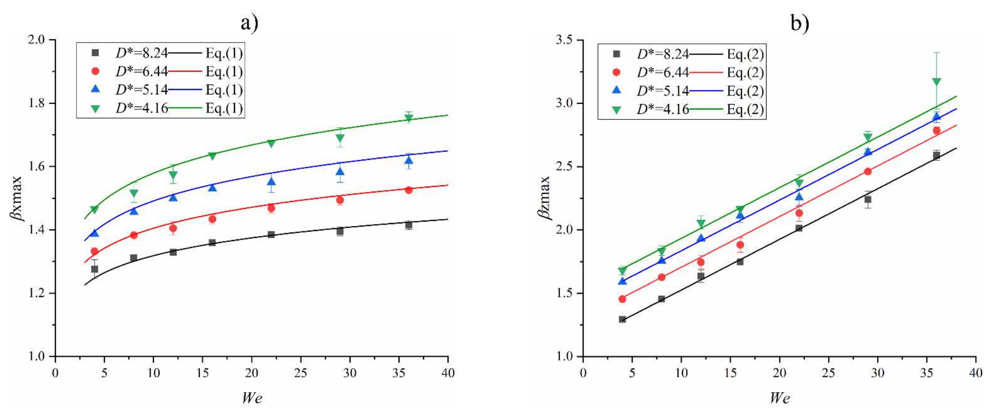

Fig.4. Diagram shows the maximum spread diameter of the azimuthal groove cylindrical surface. a) the Maximum spread diameter along the axial direction and b) the maximum spread diameter along the azimuthal direction.

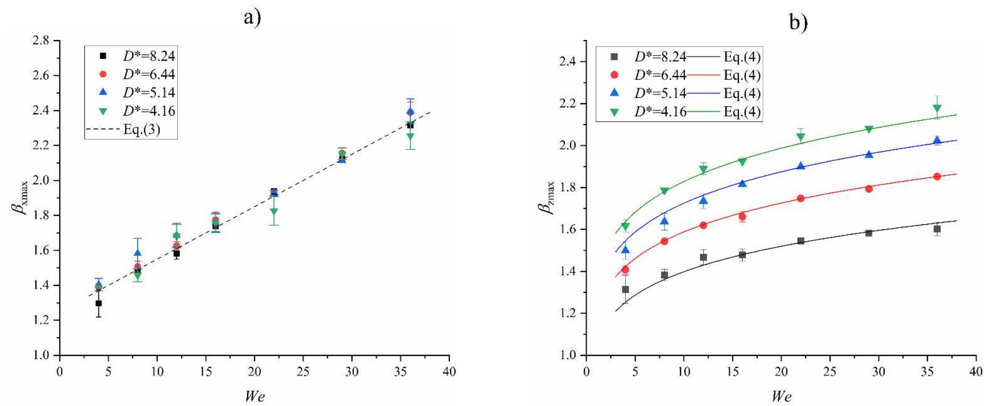

Fig.5. Diagram shows the maximum spread diameter of the axial groove cylindrical surface. a) the Maximum spread diameter along the axial direction and b) the maximum spread diameter along the azimuthal direction.

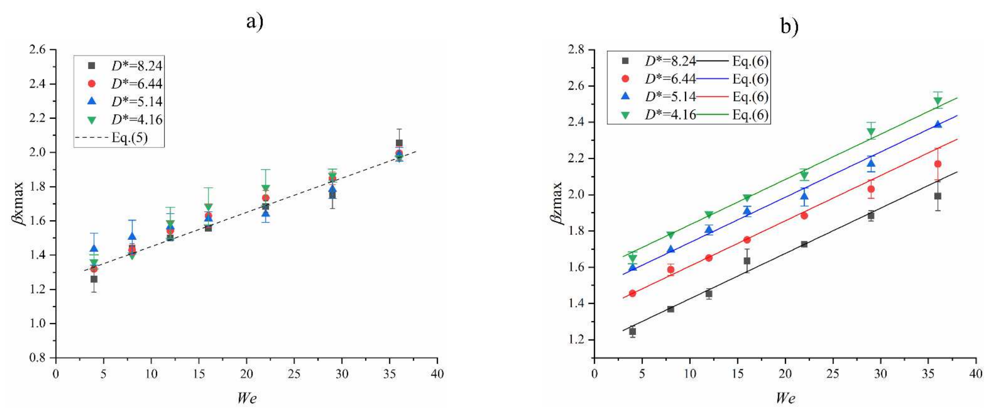

Fig.6. The diagram shows the cylindrical pillar maximum spread diameter. a) the Maximum spread diameter along the axial direction and b) the maximum spread diameter along the azimuthal direction.

B: Droplet splash

The droplet splash threshold critical line is shown in Fig.7. Corresponding to the complete rebound, the droplet splash Weber number was more significant on the cylindrical superhydrophobic surface. The splash threshold was slightly lower on the cylindrical superhydrophobic surface with structure. This is because the cylindrical superhydrophobic surface with structure increased the instability and perturbations of the droplet during the collision. The droplets are more likely to breakup and splash at a small Weber number. To better show the splash phenomenon of different structures and the difference in splash morphologies, a high-speed camera is used to capture the basic process of droplet splashing from the front view, side view, and cross view. Fig.8 shows the splash morphology at D^* =5.14. As shown in Fig. 8a, when the weber number is 80, splashing on the cylindrical superhydrophobic surface did not occur compared with other structural superhydrophobic surfaces (as shown in Fig 8c, 8d, 8e). However, when the weber number is 120 (as shown in Fig8b), splashing would occur, indicating that splashing on the cylindrical superhydrophobic surface requires higher kinetic energy. Due to the topological structure of the cylinder, the droplets would gain more kinetic energy in the azimuthal direction, and the droplets would preferentially splash in the azimuthal direction. As shown in Fig 8b, the droplet from the cross view would first spread into an oval, and fingers gradually form at the periphery of the liquid lamella (0-10ms), which is caused by the R-T instability (the higher the impact velocity and the larger the droplet size, the more the droplet rim instability. The finger shapes would appear at the edge of the droplet) of the droplet. Then the droplet would breakup and recede into a strip.[37] In the azimuthal direction (side view), the droplet would spread along the surface of the circle (0-7.5ms). When the maximum spreading diameter is reached, the inertial force overcomes the liquid's surface tension and viscous force, and the droplet begins to breakup under inertial force and gravity (10ms). In addition, in the axial direction (front view), splashing does not appear.

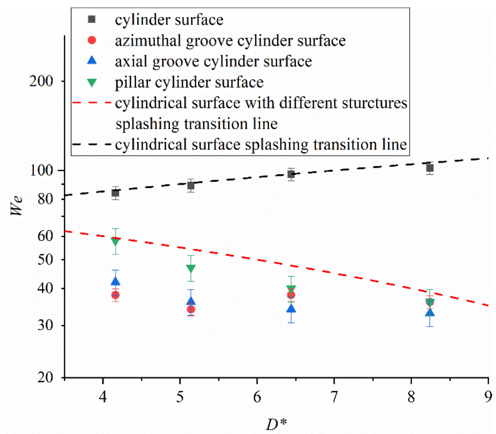

Fig.7. Diagram of the *We-D**, splash threshold of cylindrical superhydrophobic surfaces with a different structure. The black and red dashed lines represent the critical threshold line of the cylindrical superhydrophobic surface and the cylindrical superhydrophobic surface with structure, respectively.

As shown in the cross view in Fig 8c, the liquid droplets would spread out into a similar elliptical shape on azimuthal groove cylindrical superhydrophobic surface. Still, there would be jet-like fine waves (2.5ms) on both sides of the droplets, which are similar to jet flow. In the azimuthal direction (side view), unlike Fig. 8b, the droplets did not spread along the cylindrical surface but spread in a level wing-like (0-7.5ms). The droplet had a large horizontal velocity, and its spread angle was ~ 180°. Then the wings on both sides fall slowly due to gravity (12.5ms-22.5ms), and the droplet overcomes the surface tension and viscous force and splashes to both sides (15ms). In the axial direction (front view), the droplet is pinned to the substrate surface by the structure, which prevents the droplet from spreading and splashing. This is because the viscous force of the liquid caused the droplets to pin to the surface of the substrate.

The splashing of the axial groove cylindrical superhydrophobic surface is shown in Fig.8d. From the cross view, the droplet spreads and appears jet-like fine waves on the left and right sides (0-2.5ms). At 7.5ms, the droplet began to shrink and appeared as a cross shape (12.5ms), and the droplet broke into multiple satellite droplets (22.5ms). In the axial direction (front view), the droplet had an upward lift on both sides (7.5ms) and then appeared as a level wing-like (12.5ms) with a spreading angle of 180°. Under the inertial force, the middle part of the droplet bounces upward with the remaining energy.

As shown in Fig. 8e, the droplet perturbation and instability would be more pronounced on the pillar cylindrical surface. When the droplet reaches maximum spreading diameter (2.5ms), splashing occurs in both axial and azimuthal, forming a small satellite droplet (7.5ms), and the middle part of the droplet is pinned to the substrate surface (12.5ms-22.5ms).

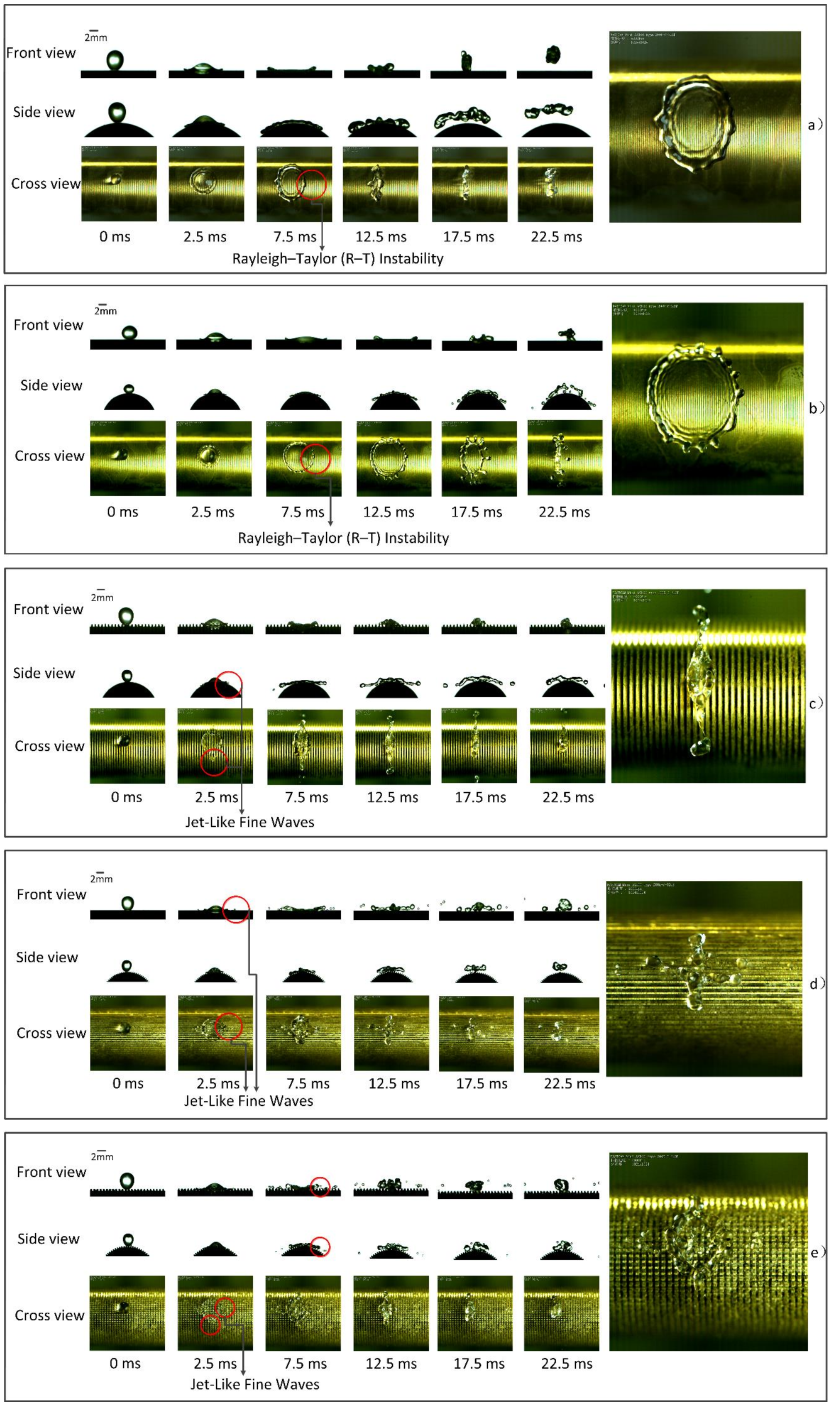
2mm
Front view
Side view
Cross view
0 ms
2.5 ms
7.5 ms
12.5 ms
17.5 ms
22.5 ms
Rayleigh–Taylor (R–T) Instability
a)
b)
Jet-Like Fine Waves
c)
d)
e)

Fig.8. Schematic diagram of splash morphology on superhydrophobic cylindrical surfaces with different structures. a) *We*=80, *D**=5.14, rebounding off the cylindrical superhydrophobic surface, b) *We*=120, *D**=5.14, splashing of the cylindrical superhydrophobic surface, c) *We*=80 *D**=5.14 splashing of the azimuthal groove cylindrical superhydrophobic surface, d) *We*=80, *D**=5.14 splashing of the axial groove cylindrical superhydrophobic surface, e) *We*=80, *D**=5.14 splashing of the pillar cylindrical superhydrophobic surface. Each image's first, second, and third rows represent high-speed snapshots selected from the front, side, and cross views.

This horizontal wing-like phenomenon is explained in Fig.9. During the spreading process of the droplet, the edge liquid gradually separates from the substrate surface, and the three-phase contact line is transformed into a two-phase contact line. The change of the contact line would reduce the disturbance of the droplet edge on the substrate surface. At the same time, the escaping air inside the substrate was also a critical factor in determining the splashing of droplets.[4, 38] As shown in Fig. 9, the droplet spreading velocity is V_l, and the air escape velocity is V_a. When the droplet impacts the inside of the groove, the air inside the groove is squeezed out by the droplet, at this time $Va>V_l$, and the escaping air generates an upward aerodynamic force. Under the effect of aerodynamic force, the edge of the liquid film would lift up and gradually form a horizontal airfoil with an angle of ~180°.

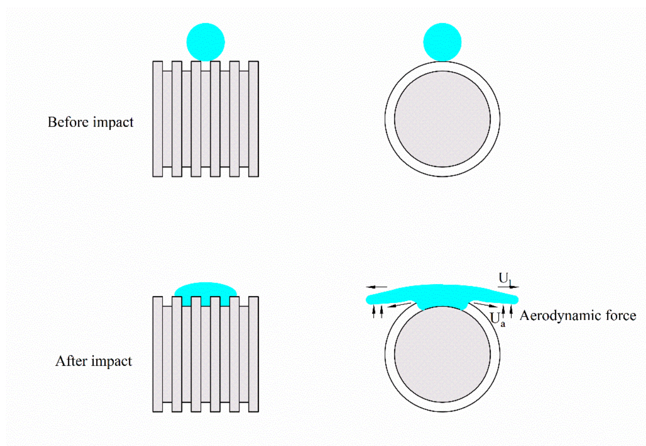

Fig.9. Schematic diagram of the level wing-like mechanism

C: Contact time

The droplet contact time is influenced by many factors, such as substrate wettability, curvature, and substrate structure. Fig. 10 compared the contact time of the cylindrical superhydrophobic surfaces with different structures at *D**6.44. In a previous study, it was found that the receding speed of droplets during spreading can be expressed as $v_r \sim (\sigma / \rho\delta)^{1/2}$ [24], where the average thickness of the film is the end of spreading. Therefore, the contraction time can be expressed as $t_r = r / (\sigma / \rho\delta)^{1/2}$, and the contact time scale can be expressed as $\tau = \sqrt{\rho r_0^3 \sigma}$.[24, 39] Thus, the contact time scale τ is used in this experiment, and the dimensionless time $t_{nc} = t_c / \tau$ is determined, where t_c is the total time from the drop touching the substrate surface to leaving the surface. As shown in Fig.10, with the increase of Weber number (0<*We*<17), the contact time would decrease, indicating that the greater the impacting velocity, the lower the contact time. With the increase of Weber number (17<*We*<70), the contact time tends to be constant, which was independent of the droplet's impact velocity. Moreover, the contact time also was different on cylindrical superhydrophobic surfaces with different structures. The contact time of the axial groove cylindrical surface was the largest, followed by the cylindrical pillar surface, cylindrical surface, and azimuthal groove cylindrical surface, respectively.

Because of the topological structure of the cylinder, the droplets spread out into an elliptic shape during the collision, the liquid film thickness could be expressed as $\delta \sim r_0^3 / \beta_{a\max}\beta_{z\max}$,[22] the retraction speed could be expressed $t_{nc} \sim (\beta_{a\max} / \beta_{z\max})^{1/2}\tau$.[19] In theory, when $\beta_{z\max}/\beta_{a\max}$ reached maximum, the contact time was minimum. The relative ratio of the maximum azimuthal non-dimension spreading diameter, and the maximum axial non-dimension spreading diameter is used to measure the strength of the maximum spreading diameter in different directions, as shown in Fig. 10b. With the increase of Weber number ($0<We<36$), it was found that, the value of $\beta_{z\max}/\beta_{a\max}$ would increases on the azimuthal groove cylindrical superhydrophobic surface, the value of $\beta_{z\max}/\beta_{a\max}$ remains unchanged on the pillar cylindrical superhydrophobic surface, and the value of $\beta_{z\max}/\beta_{a\max}$ would decrease on the axial groove cylindrical superhydrophobic surface. According to the relation $t_{nc} \sim (\beta_{a\max} / \beta_{z\max})^{1/2}\tau$, the contact time was the smallest on the azimuthal groove cylindrical superhydrophobic surface, followed by the pillar cylindrical superhydrophobic surface, and the axial groove cylindrical superhydrophobic surface was the largest.

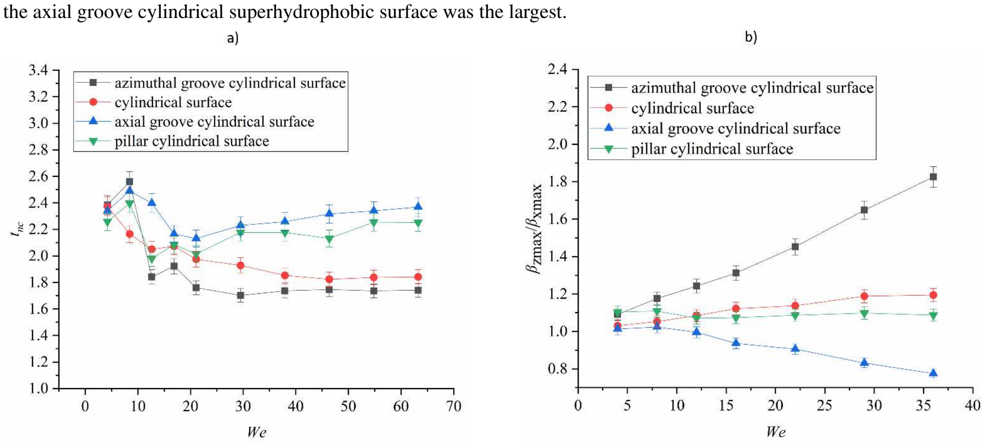

Fig.10.a) Schematic diagram of contact times of four different cylindrical superhydrophobic surfaces. b) Maximum spread diameter ratio, the ratio of maximum spreading diameter, $\beta_{a\max}$ is the maximum spreading diameter in the axial direction, $\beta_{z\max}$ is the maximum spreading diameter in the azimuthal direction.

D. Complete rebound threshold of mathematical formulation for the cylindrical superhydrophobic surface

The surface energy was difficult to simplify on the cylindrical superhydrophobic surface with structure, because droplets spreading on the surface of the superhydrophobic cylinder with structure would appear in various forms in Fig. 2b, 2b, 2d. Droplet spreading is greatly affected by surface structure. For the above reasons, complete rebound threshold of mathematical formulation for the cylindrical superhydrophobic surface with structure was not taken into account. In this section, the rebound threshold model of a droplet on the cylindrical superhydrophobic surface is considered. Based on the principle of energy conservation, a rebound threshold model of droplets on a cylindrical superhydrophobic surface is established. The threshold of complete rebound means that the droplet could fully rebound after hatted the substrate.

Based on the energy balance principle, the pre-and post-impact energies are considered to be conserved and expressed as:

$$E_{k0} + E_{s0} + E_{p0} = E_{s1} + E_{dis} + E_{p1} \tag{7}$$

where E_{k0}, E_{s0} and E_{p0} are the kinetic energy, surface energy and potential energy of the droplet before impact; and E_{s1} is the surface energy of droplet at maximum spread; E_{p0} is potential energy and E_{dis} is energy dissipated due to viscous effect after impact.

The change in potential energy is negligible in Eq.7. Because of its small magnitude compared to other energy components during spreading.[40, 41] The pre-impact kinetic energy can be expressed as

$$E_{k0} = \frac{1}{2}(\rho {U_0}^2)(\frac{\pi D_0^3}{6}) \tag{8}$$

Considering that the droplet before impact assumes a perfectly spherical shape (experiments reveal that the droplets are nearly spherical before impact; however, mild distortions are possible, which are neglected in the present case), the surface energy of the droplet pre-impact is expressed as:

$$E_{s0} = \pi D_0^2 \sigma \tag{9}$$

where σ is the surface tension of droplet.

When the droplet has complete rebound, the droplet does not splash. When the surface energy of the droplet is maximum spread, the maximum spreading film can be approximately regarded as an ellipse with a major axis l_{zmax} (in the azimuthal direction) and minor axis l_{amax} (in the axial direction), and the area of the central film is $\pi l_{zmax} l_{amax}$.[19] Therefore, the surface energy of the central film is expressed as:

$$E_{s1} \approx \pi l_{a\max} l_{z\max} \sigma (1-\cos\theta) \tag{10}$$

where θ is the static contact angle of droplet.

Since it is a cylindrical superhydrophobic surface, the effect of viscous dissipation is not considered. A collision coefficient α was added to correct the surface energy. The area of the central membrane is $\pi l_{zmax} l_{amax}$ can also be written as $\alpha\pi D^2$.

$$E_{s1} \approx \pi \alpha D^2 \sigma (1-\cos\theta) \tag{11}$$

When the kinetic energy and surface energy of the droplet before collision are greater than the surface energy of the droplet under maximum spreading, the droplet would be broken and would not have complete rebound. Substituting the energy components (8), (9), (11) into equation (7), the net energy balance equation is of the form:

$$\frac{1}{2}(\rho {U_0}^2)(\frac{\pi D_0^3}{6}) + \pi D_0^2 \sigma \approx \pi \alpha D^2 \sigma (1-\cos\theta) \tag{12}$$

Non-dimensionalzing the expression with respect to the initial surface energy of the pre-impact droplet, the relation between Weber number and D* and static contact angle (θ) is obtained as:

$$\frac{We}{12} + 1 \approx \alpha (D^*)^2 (1-\cos\theta) \tag{13}$$

which can be further expressed as a semi-empirical function of *We* as:

$$We \approx 12(\alpha (D^*)^2 (1-\cos\theta) - 1) \tag{14}$$

The collision coefficient (α) was corrected by the experimental data, the collision coefficient (α) function of the surface energy coefficient is obtained as:

$$\alpha \approx 2.45 D^{*-1.65} (3<D^*<9) \tag{15}$$

The collision coefficient function error is the experimental and fitting error, and the total error is about 8%.

The cylindrical superhydrophobic surface semi-empirical formula for complete rebound is obtained as:

$$We \approx 12(2.45 (D^*)^{0.35} (1-\cos\theta) - 1) \quad (3<D^*<9) \tag{16}$$

The semi-empirical formula has a good coincidence with the experimental data, as shown in Figure 11. The complete rebound threshold could be well predicted on the cylindrical superhydrophobic surface.

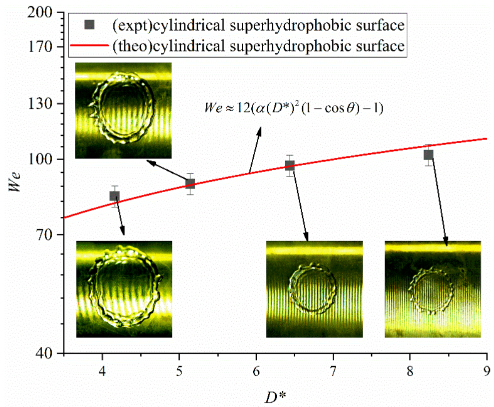

Fig.11.Comparison of experimental (expt) value and theoretical (theo) function of complete rebound threshold for various D^* and We conditions on cylindrical superhydrophobic surface.

CONCLUSIONS

In this paper, the dynamic behavior of droplets impacting cylindrical superhydrophobic surfaces with different structures is experimentally investigated. The effects of D^*, Weber number, surface structure on droplet mode (rebound, splash), recovery coefficient, contact time, and other parameters were studied. The main results are as follows:

1. The rebounding and splashing thresholds of cylindrical superhydrophobic surfaces with different structures are experimentally studied. It is found that the rebound and splash threshold is the largest on the cylindrical superhydrophobic surface, and the rebound threshold is lower on the cylindrical superhydrophobic surface with structure. Based on the principle of energy conservation, a semi-empirical mathematical model is constructed for the complete rebound of cylindrical superhydrophobic surface. The structure of the substrate surface increases the instability and oscillation of the droplet in the collision process, and the threshold of rebound and splash decreases. Meanwhile, the change of D^* will also affect the threshold of rebound and splash.
2. In the study of the maximum spreading diameter, the maximum spreading diameter in the perpendicular direction to the groove structure is inhibited during the spreading process of the droplet, and the maximum spreading diameter is promoted in the parallel direction to the groove structure. Here, the maximum spreading diameter is obtained on cylindrical superhydrophobic surfaces with different structures. In addition, a new phenomenon is discovered (level wing-like). Due to the aerodynamic force, a fine wave jet is generated to form the level wing-like further. Under certain conditions, this level wing-like is beneficial to reduce contact time.
3. The contact time of the droplet impacting different structures is compared. The contact time firstly decreases with the increase of Weber's number. After the Weber number reaches a specific value, the contact time remains unchanged with the increase of the Weber number ((the contact time is independent of the impact velocity), and the contact time on the cylindrical surface of the azimuthal groove cylindrical superhydrophobic surface is the lowest.

The dynamic behavior of cylindrical superhydrophobic surfaces with different structures is considered in the paper. But the effect of structure size on droplet dynamic behavior is not considered, which is important in subsequent studies.

ACKNOWLEDGEMENTS

This work was supported by the Excellent Youth Natural Science Foundation of Zhejiang Province, China (LR21E060001) and the National Natural Science Foundation of China with Grant Nos.11872352.

DATA AVAILABILITY STATEMENT

The data that support the findings of this study are available from the corresponding author upon reasonable request.

REFERENCES

1. Y. Wang, andL. Bourouiba, "Unsteady sheet fragmentation: droplet sizes and speeds," Journal of Fluid Mechanics **848**, 946 (2018).
2. D. Sivakumar, et al., "Spreading behavior of an impacting drop on a structured rough surface," Physics of Fluids **17**, 100608 (2005).
3. M. Song, et al., "Reducing the contact time using macro anisotropic superhydrophobic surfaces — effect of parallel wire spacing on the drop impact," NPG Asia Materials **9**, e415 (2017).
4. L. Xu, "Liquid drop splashing on smooth, rough, and textured surfaces," Phys Rev E Stat Nonlin Soft Matter Phys **75**, 056316 (2007).
5. C. Josserand, andS. T. Thoroddsen, "Drop Impact on a Solid Surface," Annual Review of Fluid Mechanics **48**, 365 (2016).
6. H. Li, et al., "Spontaneous droplets gyrating via asymmetric self-splitting on heterogeneous surfaces," Nat Commun **10**, 950 (2019).
7. N. Farhat, et al., "Numerical Study of the Wetting and Mobility of Liquid Droplets on Horizontal and Inclined Flat and Microgrooved Surfaces," Procedia Engineering **105**, 576 (2015).
8. C. Clanet, et al., "Maximal deformation of an impacting drop," Journal of Fluid Mechanics **517**, 199 (2004).
9. R. D. Schroll, et al., "Impact of a viscous liquid drop," Phys Rev Lett **104**, 034504 (2010).
10. A. Bordbar, et al., "Maximum Spreading and Rebound of a Droplet Impacting onto a Spherical Surface at Low Weber Numbers," Langmuir **34**, 5149 (2018).
11. B. Emami, et al., "Predicting longevity of submerged superhydrophobic surfaces with parallel grooves," Physics of Fluids **25**, (2013).
12. S. Gogte, et al., "Effective slip on textured superhydrophobic surfaces," Physics of Fluids **17**, (2005).
13. S. Khanzadeh Borjak, et al., "Experimental Investigation of Water Droplet Impact on the Electrospun Superhydrophobic Cylindrical Glass: Contact Time, Maximum Spreading Factor, and Splash Threshold," Langmuir **36**, 13498 (2020).
14. M. Andrew, et al., "Variation of the Contact Time of Droplets Bouncing on Cylindrical Ridges with Ridge Size," Langmuir **33**, 7583 (2017).
15. V. Vaikuntanathan, andD. Sivakumar, "Transition from Cassie to impaled state during drop impact on groove-textured solid surfaces," Soft Matter **10**, 2991 (2014).
16. N. D. P. Laxman K. Mallaa, Rajneesh Bhardwajb, Adrian Neildc, "Droplet Bouncing and Breakup during Impact on Microgrooved Surface," **33**, 9620 (2017).
17. Y. Liu, et al., "Pancake bouncing on superhydrophobic surfaces," Nat Phys **10**, 515 (2014).
18. G. Khurana, et al., "Post-collision hydrodynamics of droplets on cylindrical bodies of variant convexity and wettability," Physics of Fluids **31**, (2019).
19. H. Zhang, et al., "Dynamic behavior of water drops impacting on cylindrical superhydrophobic surfaces," Physics of Fluids **31**, (2019).
20. H. Zhang, et al., "Asymmetric splash and breakup of drops impacting on cylindrical superhydrophobic surfaces," Physics of Fluids **32**, (2020).
21. Z. Jin, et al., "The impact and freezing processes of a water droplet on different cold cylindrical surfaces," International Journal of Heat and Mass Transfer **113**, 318 (2017).
22. Y. Liu, et al., "Symmetry breaking in drop bouncing on curved surfaces," Nat Commun **6**, 10034 (2015).

23. M. Abolghasemibizaki, andR. Mohammadi, "Droplet impact on superhydrophobic surfaces fully decorated with cylindrical macrotextures," J Colloid Interface Sci **509**, 422 (2018).
24. M. Abolghasemibizaki, et al., "Towards the shortest possible contact time: Droplet impact on cylindrical superhydrophobic surfaces structured with macro-scale features," J Colloid Interface Sci **521**, 17 (2018).
25. S. R. Mishra, et al., "Elasto-hydrodynamics of non-Newtonian droplet collision with convex substrates," Physics of Fluids **33**, (2021).
26. D. Khojasteh, et al., "Curvature effect on droplet impacting onto hydrophobic and superhydrophobic spheres," International Journal of Computational Fluid Dynamics **31**, 310 (2017).
27. Q. Li, et al., "Deformation and breakup of a liquid droplet past a solid circular cylinder: a lattice Boltzmann study," Phys Rev E Stat Nonlin Soft Matter Phys **90**, 043015 (2014).
28. Y. Wang, "Numerical study of a droplet impact on cylindrical objects: Towards the anti-icing property of power transmission lines," Applied Surface Science **516**, (2020).
29. Y. Wang, et al., "Droplet impact on cylindrical surfaces: Effects of surface wettability, initial impact velocity, and cylinder size," J Colloid Interface Sci **578**, 207 (2020).
30. X. Liu, et al., "Numerical research on the dynamic characteristics of a droplet impacting a hydrophobic tube," Physics of Fluids **29**, (2017).
31. L.-Z. Zhang, et al., "Re-touch rebound patterns and contact time for a droplet impacting a superhydrophobic cylinder," Journal of the Taiwan Institute of Chemical Engineers **126**, 359 (2021).
32. D. Bartolo, et al., "Bouncing or sticky droplets: Impalement transitions on superhydrophobic micropatterned surfaces," Europhysics Letters (EPL) **74**, 299 (2006).
33. X. Yan, et al., "Laplace Pressure Driven Single-Droplet Jumping on Structured Surfaces," ACS Nano **14**, 12796 (2020).
34. Y. H. Yeong, et al., "Drop impact and rebound dynamics on an inclined superhydrophobic surface," Langmuir **30**, 12027 (2014).
35. R. B. Nagesh D. Patil, Atul Sharma, "Droplet impact dynamics on micropillared hydrophobic surfaces," Experimental Thermal and Fluid Science **74**, 195 (2016).
36. Z. Yuan, et al., "Directional rebounding of a droplet impinging hydrophobic surfaces with roughness gradients," International Journal of Multiphase Flow **138**, (2021).
37. X. Huang, et al., "Axisymmetric rim instability of water droplet impact on a super-hydrophobic surface," Physics of Fluids **30**, (2018).
38. L. Xu, et al., "Drop splashing on a dry smooth surface," Phys Rev Lett **94**, 184505 (2005).
39. C. C. D. Richard, and D. Quéré, "Contact time of a bouncing drop," Nature **417(6891)**, 811 (2002).
40. S. Mitra, et al., "On wetting characteristics of droplet on a spherical particle in film boiling regime," Chem Eng Sci **149**, 181 (2016).
41. M. Pasandideh‐Fard, et al., "Capillary effects during droplet impact on a solid surface," Physics of Fluids **8**, 650 (1996).

APPENDIX

A: Summary of the experimental and numerical simulation for the droplet impact on cylindrical superhydrophobic surfaces

Table 2: List of experimental investigations and their most important findings regarding droplet impacting onto cylindrical superhydrophobic surface

Author	Dimensionless numbers	Droplet dimension or size ratio	Type of surface	Main outcomes
Zhang et al.[19]	7.5<*We*<70	0.38<*D**<7.69	Cylindrical stain steels	Asymmetric rebound and stretched breakup could effectively

			superhydrophobic surface Contact angle:156°	shorten the contact time between drops and substrates, and the reduction in contact time is affected by α more dramatically in the stretched breakup regime. $\tau_c \propto \alpha^n = (We / D^*)^n$
Zhang et al.[20]	142<*We*<720	0.38<*D**<7.69	Cylindrical stain steels superhydrophobic surface Contact angle:156°	The drop splash would preferentially occur in the axial direction and propose two disparate splash thresholds referring to Weber number We and diameter ratio D* in the azimuthal and axial directions, respectively. Hence, the normal Weber number in the axial direction and azimuthal direction can be expressed as $We_c\|z = \begin{cases} We_{c0} \dfrac{D^{*2}}{D^{*2} - \frac{1}{3}} (D^* > 1) \\ \dfrac{3}{2} \dfrac{We_{c0}}{D^*} (0 < D^* \le 1) \end{cases}$ $We_c\|x = \begin{cases} We_{c0} (D^* > 1) \\ \dfrac{We_{c0}}{D^*} (0 < D^* \le 1) \end{cases}$
Khurana et al.[18]	36<*We*<89	0.57< *D**<1.67	Stainless steel rods superhydrophobic and hydrophilic surface Contact angle:135°±2°and 45°±2°	The maximum wetting fraction is attained faster for lower diameter ratios. Moreover, in the case of SH surfaces, the wetting fraction reduces significantly, whereas the spread factor remains comparable to that of hydrophilic surfaces. The temporal evolution of the film thickness at the north pole of the target has been presented. $h^*(t) = \dfrac{R_{cyl}^2}{2R_{cyl} D_d + D_d{}^2 \tau - D_d{}^2}$
Liu et al.[22]	7.9<*We*<70	2.1<*D**<6.9	Solid circular cylindrical	The novel phenomenon results from an asymmetric momentum and

			superhydrophobic surface Contact angle:163.4°±2.4	mass distribution that allows for preferential fluid pumping around the drop rim. The asymmetry of the bouncing leads to ~40% reduction in contact time.
Abolghasemibizaki et al.[23, 24]	10<We<100	1<D^*<3.5	Borosilicate glass tubes with macro-scale features Contact angle:165.8°±2.6°	It was found that regardless of the droplet location of the contact point, when the kinetic energy of the drop is sufficient to completely wet the ridges, the contact time reduces ~13% as the consequence of ~20% faster retraction.
Khanzadeh Borjak et al.[13]	27<We<161	3.5<D^*<16	Cylindrical glasses Contact angle: 158°±2.6°	The contact time on the cylindrical surface is up to 50% less than the flat one.
This study	3<We<150	3<D^*<9	Cylindrical brass Contact angle: 158°±2.5°	A new phenomenon is discovered (level wing-like). This level wing-like is beneficial to reduce contact time. A complete rebound threshold semi-empirical model is constructed for cylindrical superhydrophobic surfaces. $We \approx 12(\alpha(D^*)^2(1-\cos\theta)-1)$ The collision coefficient (α) is used to correct the surface energy of droplet spreading. It's a function of D^*. $\alpha \approx 2.45 D^{*-1.65}$ (3<D^*<9)

Table 3: List of numerical investigations and their most important findings regarding droplet impacting onto cylindrical superhydrophobic surface

Authors	Method	Dimensionless numbers	Droplet dimension or size ratio	Type of surface	Main outcomes
Wang et al.[28, 29]	particle-base mesh-free numerical	No define	The number density of cluster for droplet is 9, and the radius of the droplet is 12	Cylindrical surface	Contact time is not a monotonic function of the impact velocity; it can increase first with the increase of impact velocity, then decrease with the further increase of impact velocity.
Khojasteh et al.[26]	Level-Set Method	Weber number 5<We<30	2<D^*<4	Spheres surface Contact angle:163°	The contact time of droplet is on the spreading diameter, almost same for flat surface and sphere surface with a higher value of D^*.

Li et al.[27]	Improved interparticle -potential lattice Boltzmann method	No define	Droplet radius:50 lattice units. cylinder with radius:40 lattice units	Solid circular Contact angle: 70° or 170°	Breakup and no breakup are determined by the eccentric ratio (β). The viscosity ratio strongly affects the shape of the daughter droplets, breakup positions, and thickness of the deposited liquid film. The wettability has an important effect on the dynamic behavior of the droplet, the deposition place of liquid film, and the passing time of the droplet passing cylinder.
Liu et al.[30]	A coupled level set and volume-of-fluid method.	No define	$0.2<D^*<3$	Cylindrical surface Contact angle: 107°,120°,135°,153°	The worse the surface wettability is, the easier the liquid film rebounds. The maximum spreading diameter increases with the increase of the impact velocity.
Zhang et al.[31]	Lattice Boltzmann method	$10<We<45$	$0.57<D^*<1.43$	Contact angle 165°	The rebound dynamics and contact times for the first and second bouncing both strongly depend on a combined dimensionless parameter, $\alpha=We/R^*$
Andrew et al. [14]	Lattice Boltzmann method	$10<We<39$	$0.4<D^*<2.5$	Contact angle 165°	Drops bounce upon cylindrical ridges varies substantially as the size of the ridge is changed. Increasing the width of the ridge has opposite effects upon the contact time. The anisotropic curvature of the surface is responsible for the contact time reduction.

494

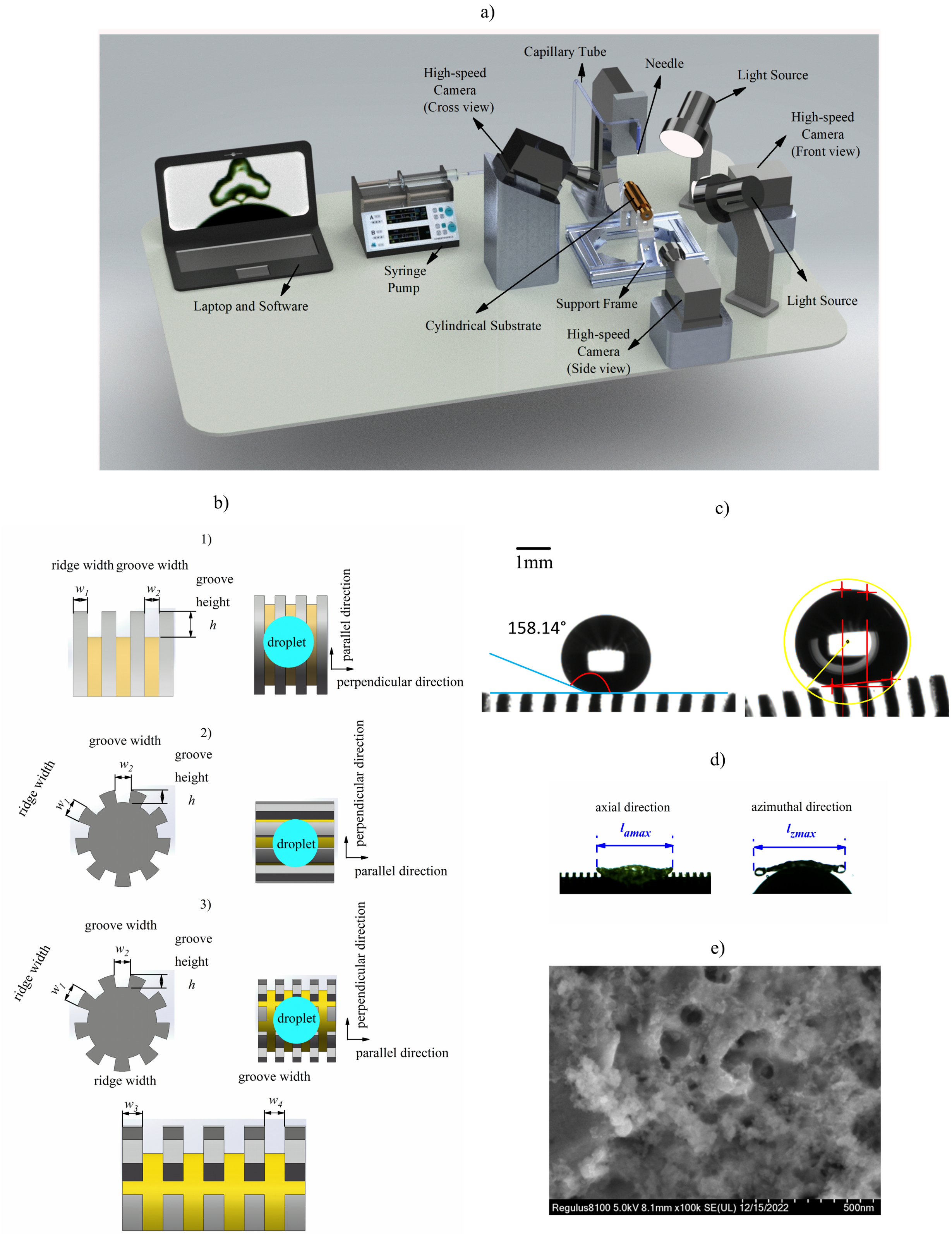
a)
Capillary Tube
Needle
Light Source
High-speed
Camera
(Cross view)
High-speed
Camera
(Front view)
Syringe
Pump
Laptop and Software
Support Frame
Light Source
Cylindrical Substrate
High-speed
Camera
(Side view)
b)
1)
ridge width groove width
groove
height
h
droplet
parallel direction
perpendicular direction
2)
groove width
ridge width
groove
height
h
droplet
perpendicular direction
parallel direction
3)
groove width
ridge width
groove
height
h
droplet
perpendicular direction
parallel direction
ridge width
groove width
c)
1mm
158.14°
d)
axial direction
azimuthal direction
l_{amax}
l_{zmax}
e)
Regulus8100 5.0kV 8.1mm x100k SE(UL) 12/15/2022
500nm

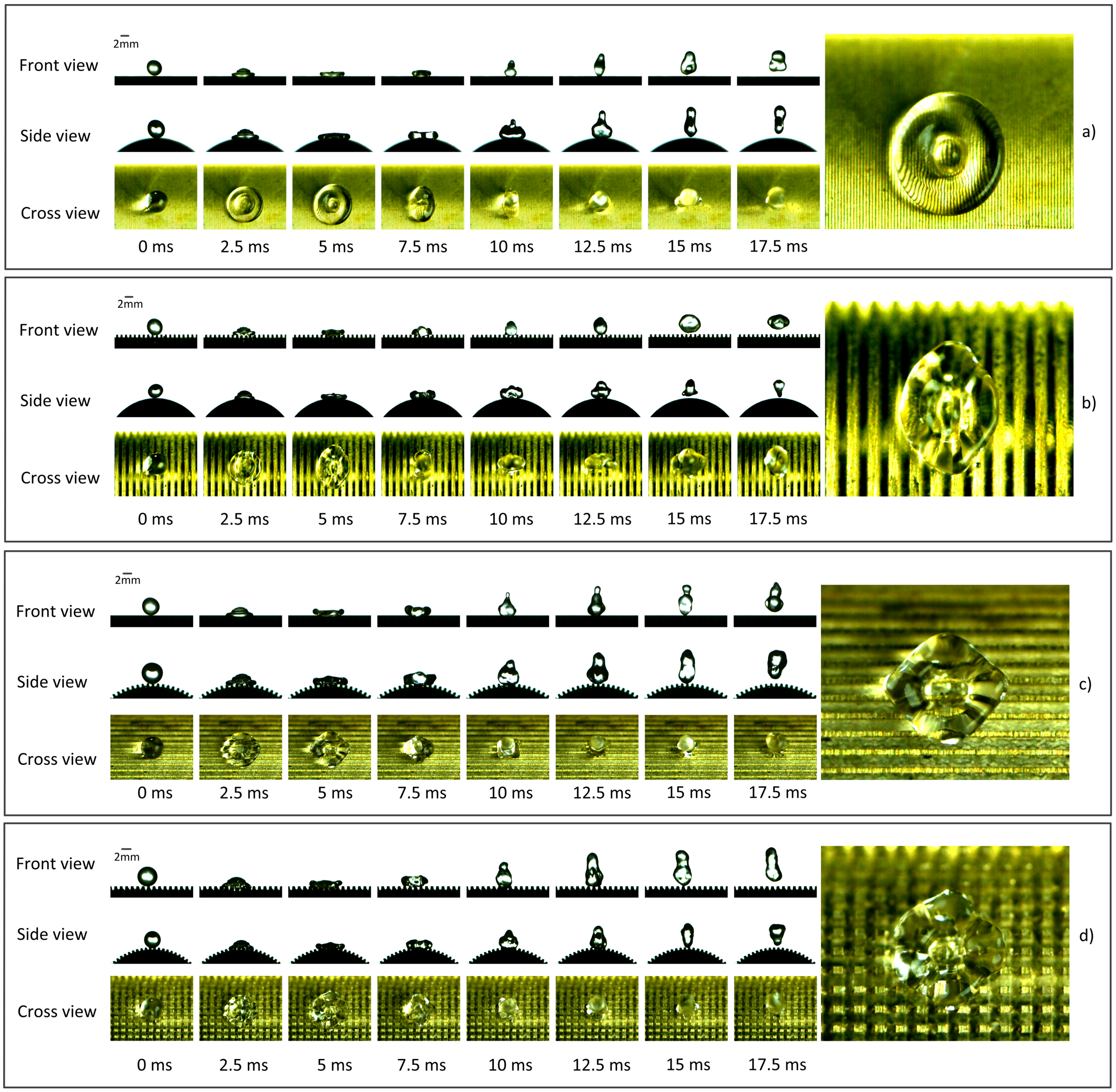
2mm
Front view
Side view
Cross view
0 ms
2.5 ms
5 ms
7.5 ms
10 ms
12.5 ms
15 ms
17.5 ms
a)
b)
c)
d)

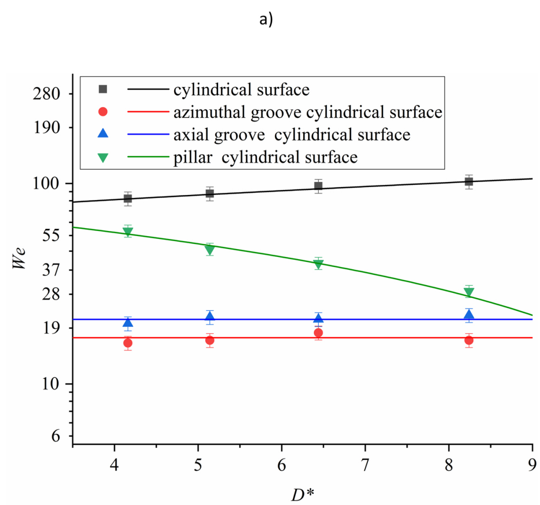
a)
cylindrical surface
azimuthal groove cylindrical surface
axial groove cylindrical surface
pillar cylindrical surface
We
D*
280
190
100
55
37
28
19
10
6
4
5
6
7
8
9

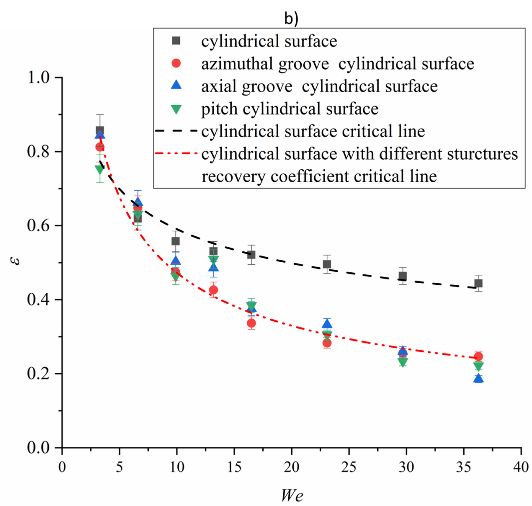
b)
cylindrical surface
azimuthal groove cylindrical surface
axial groove cylindrical surface
pitch cylindrical surface
cylindrical surface critical line
cylindrical surface with different sturctures
recovery coefficient critical line
ε
We
1.0
0.8
0.6
0.4
0.2
0.0
0
5
10
15
20
25
30
35
40

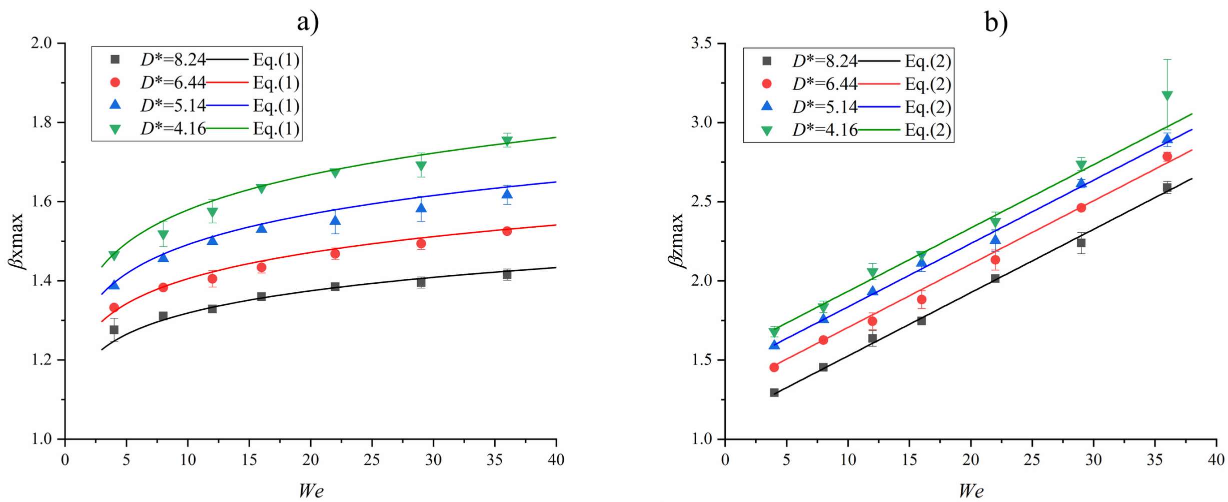
a)
b)
D*=8.24 Eq.(1)
D*=6.44 Eq.(1)
D*=5.14 Eq.(1)
D*=4.16 Eq.(1)
βxmax
D*=8.24 Eq.(2)
D*=6.44 Eq.(2)
D*=5.14 Eq.(2)
D*=4.16 Eq.(2)
βzmax
We
We

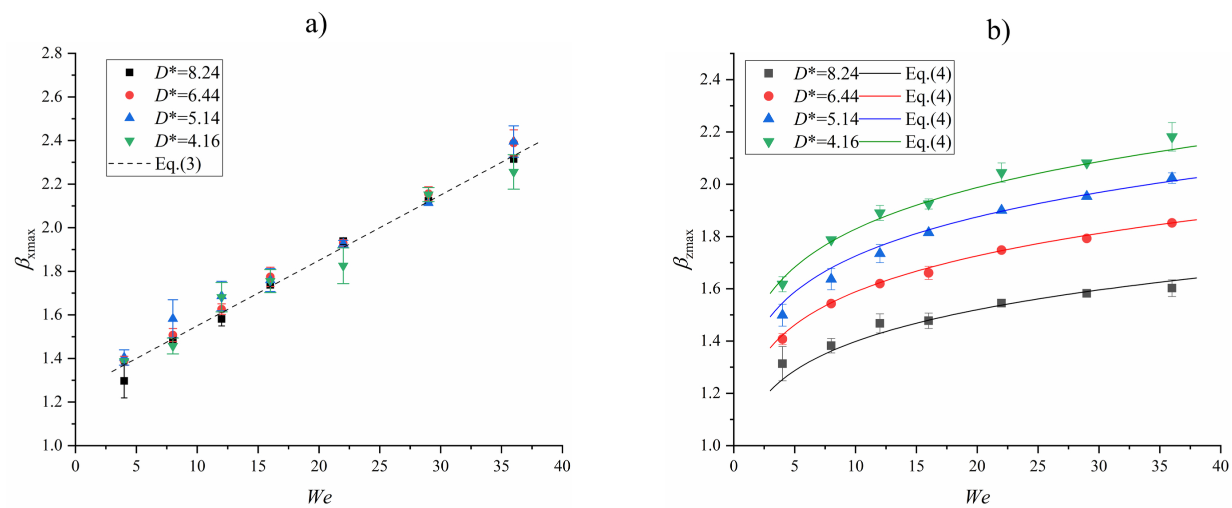
a)
D*=8.24
D*=6.44
D*=5.14
D*=4.16
Eq.(3)
βxmax
We
b)
D*=8.24 Eq.(4)
D*=6.44 Eq.(4)
D*=5.14 Eq.(4)
D*=4.16 Eq.(4)
βzmax
We

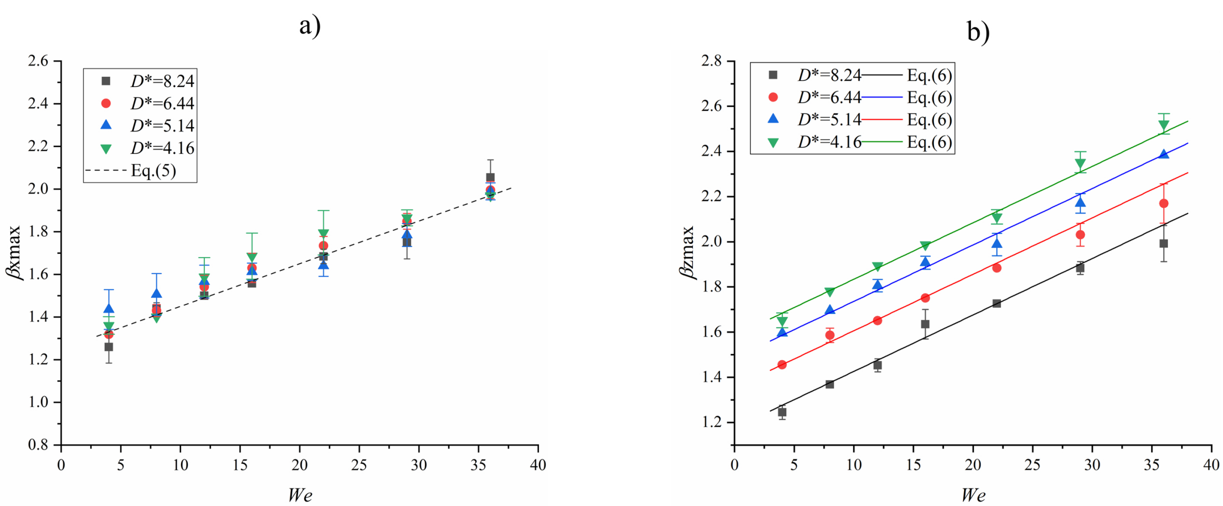
a)
D*=8.24
D*=6.44
D*=5.14
D*=4.16
Eq.(5)
βxmax
We
b)
D*=8.24 Eq.(6)
D*=6.44 Eq.(6)
D*=5.14 Eq.(6)
D*=4.16 Eq.(6)
βzmax
We

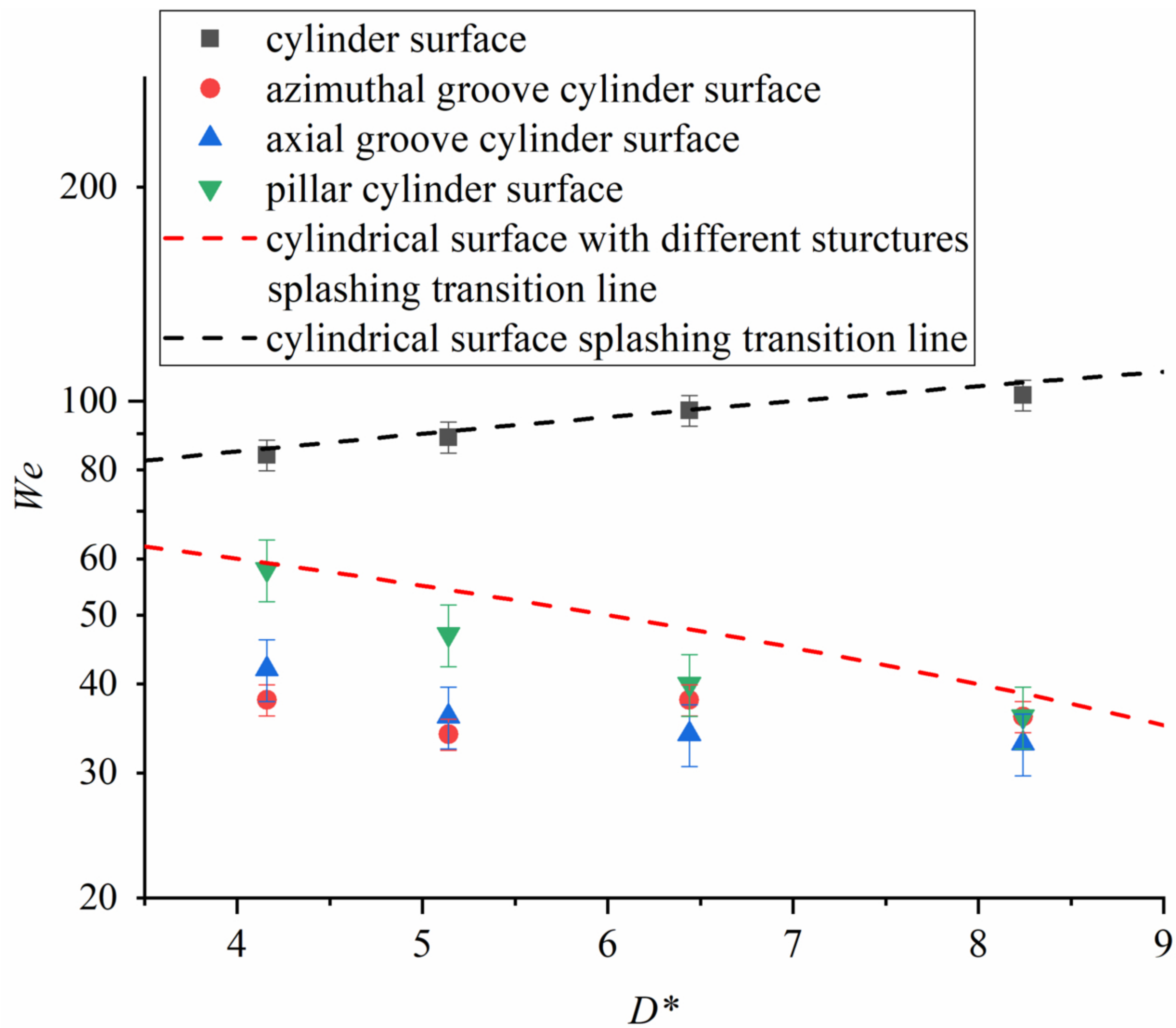
cylinder surface
azimuthal groove cylinder surface
axial groove cylinder surface
pillar cylinder surface
cylindrical surface with different sturctures splashing transition line
cylindrical surface splashing transition line
We
200
100
80
60
50
40
30
20
4
5
6
7
8
9
D*

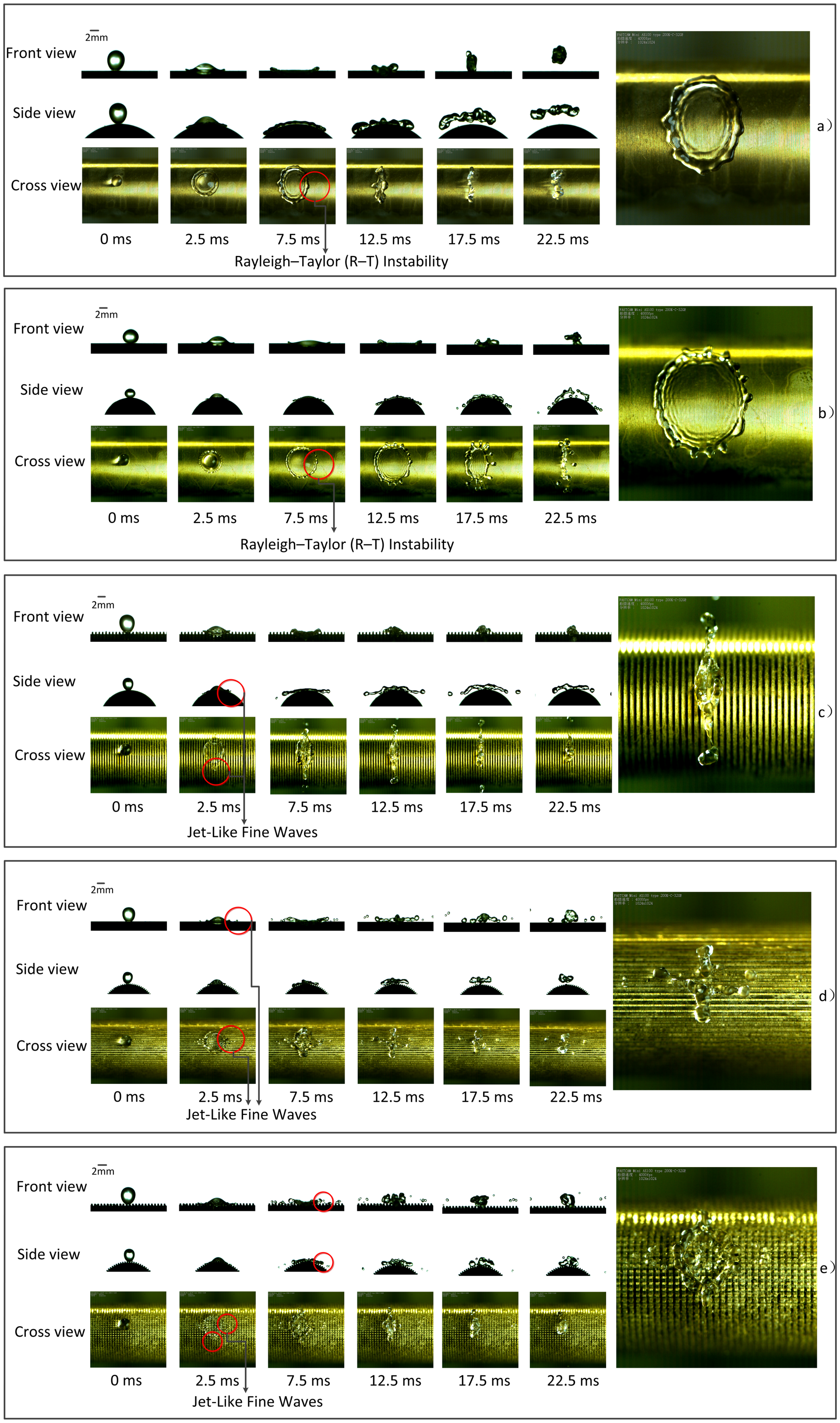
2mm
Front view
Side view
Cross view
0 ms
2.5 ms
7.5 ms
12.5 ms
17.5 ms
22.5 ms
Rayleigh–Taylor (R–T) Instability
a)
b)
Jet-Like Fine Waves
c)
d)
e)

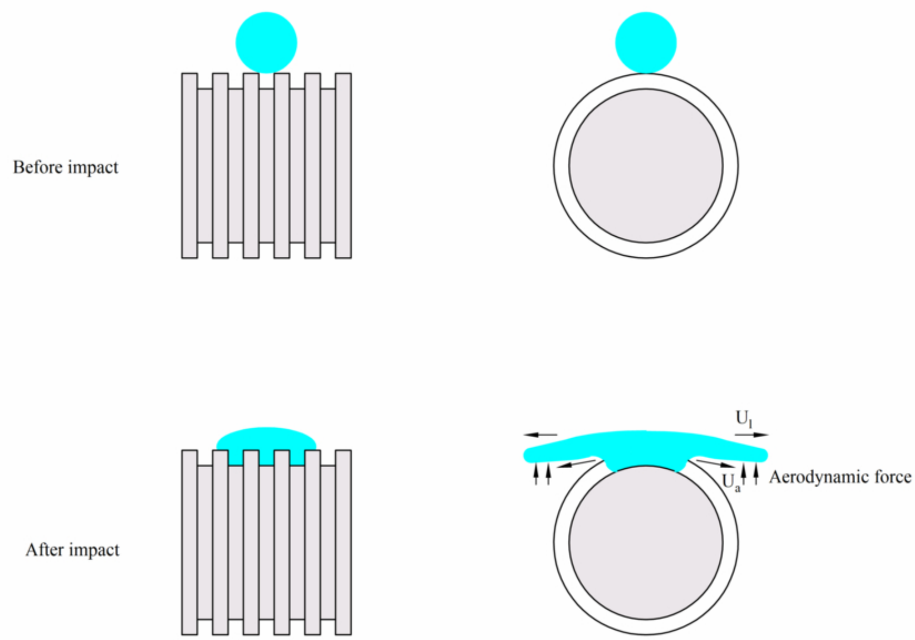
Before impact
After impact
U_l
U_a
Aerodynamic force

Author Accepted Manuscript version of the paper by Lijuan Qian et al.
in Physics of Fluids, Vol 35 (2023) DOI: http://dx.doi.org/10.1063/5.0134637

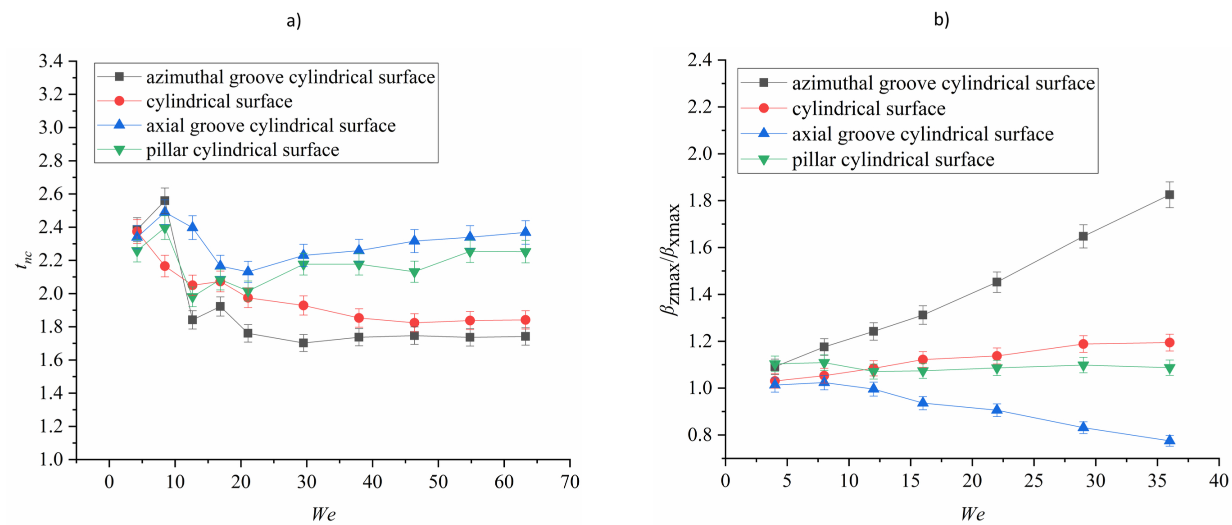

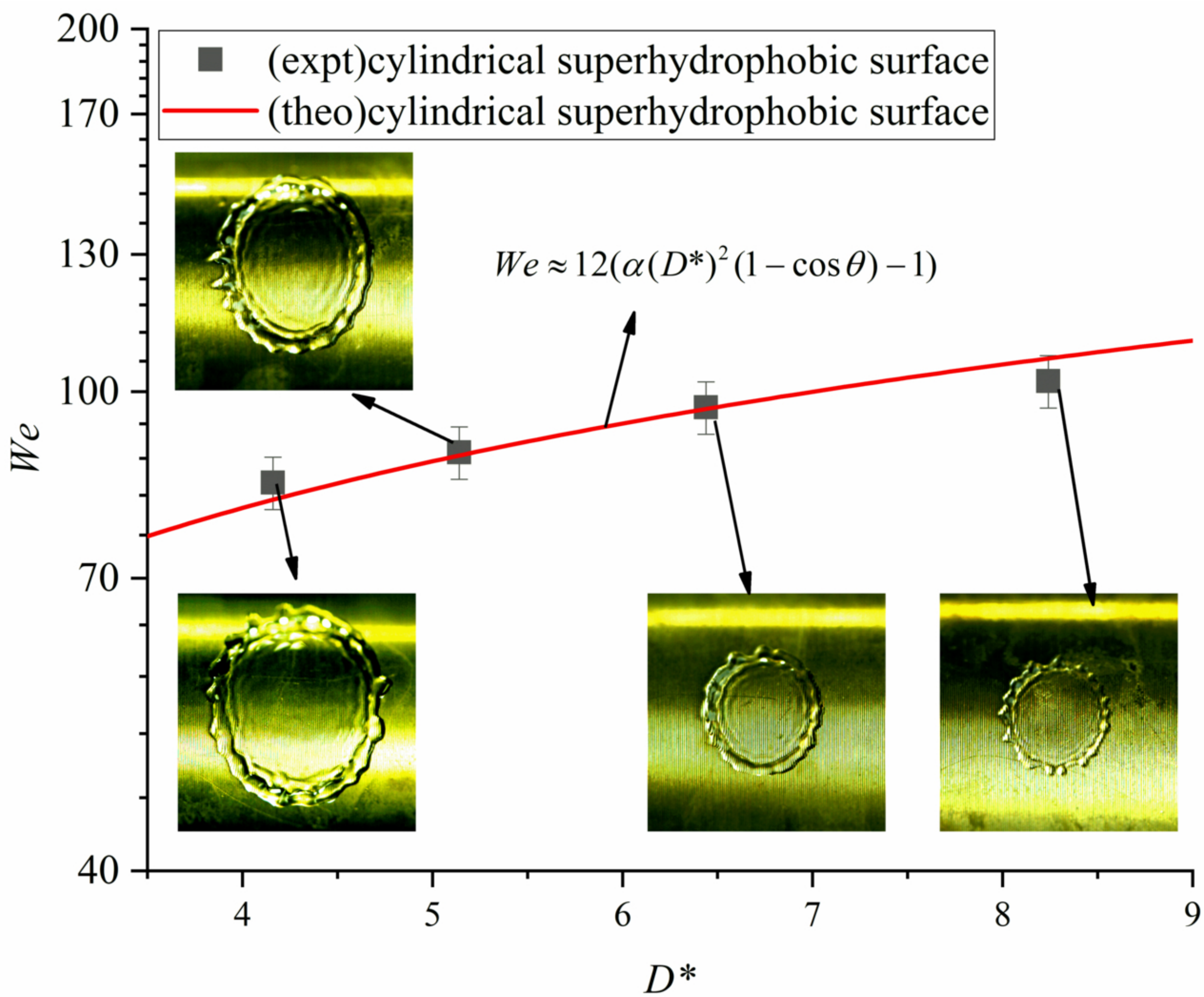
(expt)cylindrical superhydrophobic surface
(theo)cylindrical superhydrophobic surface
$We \approx 12(\alpha(D^*)^2(1-\cos\theta)-1)$
We
D*
200
170
130
100
70
40
4
5
6
7
8
9